Probing Nonadiabatic Effects in Strong-Field Tunnel Ionization

R. Boge,* C. Cirelli, A. S. Landsman, S. Heuser, A. Ludwig, J. Maurer, M. Weger, L. Gallmann, and U. Keller

Physics Department, ETH Zurich, 8093 Zurich, Switzerland

(Received 26 April 2013; published 5 September 2013)

We investigate experimentally the validity of proposed theories extending the tunneling approximation towards the multiphoton regime in strong-field ionization of helium. We employ elliptically polarized laser pulses and demonstrate how the influence of the ion potential on the released electron encoded in the measured observable provides the desired sensitivity to detect nonadiabatic effects in tunnel ionization. Our results show that for a large intensity range the proposed nonadiabatic theories contradict the experimental trends of the data, while adiabatic assumptions are confirmed.

DOI: 10.1103/PhysRevLett.111.103003 PACS numbers: 32.80.Fb, 31.15.xg, 32.80.Rm

In atomic and molecular physics, photoionization by intense low-frequency laser fields is best described by a tunneling process: the laser field bends the binding Coulomb potential of an atom forming a barrier through which the electron may tunnel out of the atom and subsequently be accelerated by the laser field. In this picture, the electron propagates through the horizontal channel [1,2] crossing the barrier without gaining any energy [Fig. 1(a)]. For weaker laser fields, multiphoton absorption may occur, where the electron is elevated into an unbound state by the absorption of multiple photons, following a vertical ionization channel within the potential energy surface [Fig. 1(a)].

Ionization rates and photoelectron distributions are described by theories developed by Perelomov, Popov, and Terentev (PPT) [3] based on Keldysh's pioneering work [4] and further summarized by Ammosov, Delone, and Krainov (ADK) [5].

The two regimes are usually distinguished by the Keldysh parameter [4] $\gamma = \omega\sqrt{2I_p}/F$ with small $\gamma \ll 1$ for tunneling and large $\gamma \gg 1$ for multiphoton ionization. Here, ω is the angular frequency of the laser field, I_p is the ionization potential of the atom, and F is the strength of the applied electric field. As shown by Keldysh in the regime with $\gamma \ll 1$, the electron experiences essentially a static field while tunneling and therefore the adiabatic condition applies [4]. Nonadiabatic effects may arise if this condition is not satisfied, especially for larger values of γ in the multiphoton regime [2].

Directly from this separation, the following question arises: at which Keldysh parameter does the transition between the two regimes occur? This issue has been widely discussed and is the subject of controversy without conclusive results [2,6]. So far, the transition is assumed to emerge around $\gamma \approx 1$, which is the value of γ corresponding to most present day experiments in the infrared wavelength range; see, for instance, [7–11] among many others. Around this value of γ significant nonadiabatic effects are expected to appear [12–14]. Nevertheless, many strong-field ionization experiments rely on adiabatic theory to interpret their results [8,9,15]. Is it justified to neglect nonadiabatic effects in current experimental regimes, and if not, what is the appropriate nonadiabatic description?

Despite much theoretical work [16,17], there are very few experimental tests of the validity of adiabatic approximations, with contradictory results [6,18]. In particular, Arissian *et al.* [6] confirmed the validity of the adiabatic approximation by comparing the experimentally measured transverse momentum spread to the ADK formula over a range of intensities. On the other hand, Shafir *et al.* [18] found that the initial velocity offset of the electron at the tunnel exit was nonzero, contradicting the adiabatic models used in [7,15], which predict zero initial velocity for the most probable electron trajectory.

However, any experimental tests of nonadiabaticity are particularly complicated, as one must often rely on the same theory that is being tested to interpret the data. Hence, the conclusions in Arissian *et al.* [6] depended on experimental calibration of intensity, which is done using an adiabatic theory that assumes zero initial velocity for the most likely trajectory. On the other hand, Shafir *et al.* [18] calibrated their experimental observable (the phase difference between the two color fields) using a model that was later to be confirmed by their experiment.

Therefore, in both experiments [6,18], the same theoretical model that was used for calibration of data was subsequently validated by the analysis of the same now- calibrated data. However, as we show in our work, assuming either adiabatic or nonadiabatic models for data calibration might give results which are consistent with adiabatic or nonadiabatic models, respectively.

To avoid this problem, in this Letter we compare experimental data over a range of γ values with adiabatic and nonadiabatic theories by selecting an observable, which is maximally sensitive to nonadiabatic effects. Our results rely on trends in the data and the conclusions are not dependent on the precise calibration of intensity. In addition, the observable used to test different theories is extracted directly from the experiment and does not rely on any theoretical assumptions, allowing for an independent test of theoretical predictions. We obtain that the

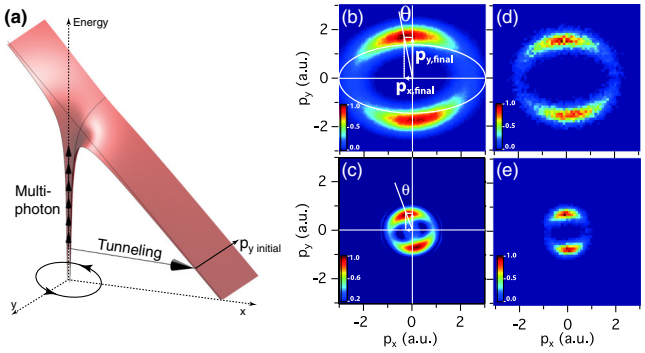

FIG. 1 (color online). (a) Potential energy surface of laser-induced ionization showing possible ionization mechanisms. (b),(c) Measured momentum distributions from strong-field ionization of helium with elliptically polarized pulses at an intensity of about 7×10^{14} and 2×10^{14} W/cm^2 respectively, with an ellipticity of $\varepsilon = 0.87$. In (b), the orientation of the polarization ellipse, with its major axis along p_x and minor axis along p_y, the definition of the final momenta $p_{x\,\mathrm{final}}$ and $p_{y\,\mathrm{final}}$, and the angular offset θ are drawn in white. (d),(e) Momentum distributions calculated under the same conditions as (b) and (c), respectively.

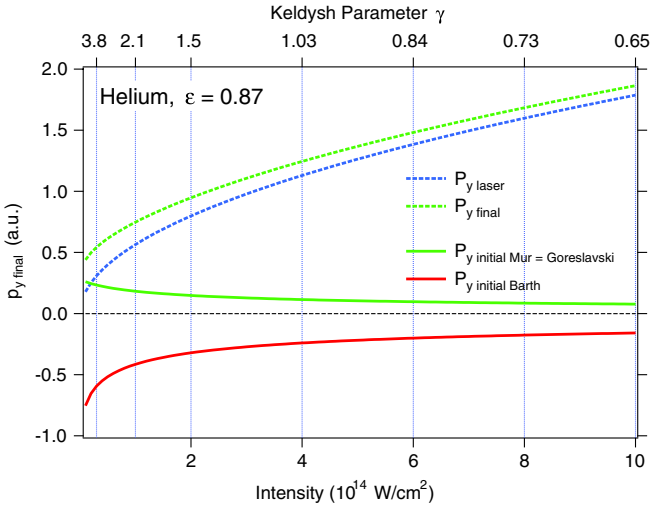

FIG. 2 (color online). Initial and final momentum of photoelectrons along the y axis according to different theories. For the definition of the momenta refer to Eq. (2). The final momentum $p_{y\,\mathrm{final}}$ (green dashed line) is the same in the nonadiabatic theories developed by Mur *et al.* [12], Goreslavski *et al.* [19], and Barth *et al.* [14]. Identical momentum offset $p_{y\,\mathrm{initial}}$ at the tunnel exit by Mur and Goreslavski (green solid line) and the momentum offset by Barth *et al.* before the tunnel barrier (red solid line).

assumption of zero velocity at the tunnel exit predicted by adiabatic models gives results that are much more consistent with our data than many currently used nonadiabatic predictions.

In the quasiclassical approximation, where sub-barrier trajectories are calculated using the imaginary-time method [3,12], minimizing the imaginary part of the action gives the most likely or ''extreme'' trajectory, corresponding to electrons found at the peak of the momentum distribution measured at the detector. The full momentum distribution is obtained from all trajectories weighted by their probability [3]. This formalism is valid for tunneling as well as for multiphoton absorption. For small γ it converges to the quasistatic case of adiabatic tunneling.

Based on this theory, approaching the nonadiabatic regime with $\gamma \approx 1$, Perelomov *et al.* [3] and, more recently, Mur *et al.* [12] proposed, due to nonadiabaticity, the presence of an additional momentum offset $p_{y\,\mathrm{initial}} \neq 0$ at the moment the electron exits the barrier. This offset is defined as the time derivative of the extreme trajectory at the moment of tunnel exit [Fig. 2, green solid line]:

$$p_{y\,\mathrm{initial}} = -i\omega \frac{dy}{d\tau}\bigg|_{\tau_0} = \frac{\varepsilon F}{\omega}\left(\frac{\sinh(\tau_0)}{\tau_0} - 1\right) > 0 \quad (1)$$

with $\tau_0 = -i\omega t_0$, where t_0 is the purely imaginary time of the sub-barrier motion and ε the ellipticity. The positive sign of $p_{y\,\mathrm{initial}}$ leads to a final momentum of

$$p_{y\,\mathrm{final}} = p_{y\,\mathrm{initial}} + p_{y\,\mathrm{laser}} = \frac{\varepsilon F}{\omega}\left(\frac{\sinh(\tau_0)}{\tau_0} - 1\right) + \frac{\varepsilon F}{\omega} = \frac{\varepsilon F}{\omega}\frac{\sinh(\tau_0)}{\tau_0} \quad (2)$$

becoming larger [Fig. 2, green dashed line] than the final momentum $p_{y\,\mathrm{laser}}$, where $p_{y\,\mathrm{laser}}$ was obtained by propagation in the laser field [Fig. 2, dashed blue line] with zero initial momentum. Furthermore, the final momentum $p_{y\,\mathrm{final}}$ is found to be in agreement with the initial offset obtained from Goreslavski *et al.* [19].

Barth *et al.* [14] also derived an initial momentum offset $p_{y\,\mathrm{initial}}$ [Fig. 2, red solid line] using the same approach. However, the offset is calculated for the moment the electron enters the barrier. Therefore, in the context of this paper we consider the initial momentum offset given by Mur *et al.*

In order to compare experiment to theory, we generate momentum distributions with semiclassical calculations, following the first two steps of the three-step model [1] including the Coulomb interaction during propagation; see Fig. 1. The ionization probability, exit point, and initial velocity are derived from quantum mechanics. Subsequently, the electron is propagated classically by solving Newton's equation of motion. To model the correct exit point and Coulomb interaction, we apply the TIPIS model [7,20], taking Stark shift and dipole effects into account. The simulations are performed for the adiabatic case without initial momentum offset and for the nonadiabatic case, where an initial momentum offset is assigned to the electron according to Eq. (1) when it is placed into the continuum at the exit of the barrier. The most convenient way to do this is to place one single electron into the continuum at the maximum of the laser pulse and to propagate it (single trajectory, ST), directly obtaining

the final momenta $p_{x\,\mathrm{final}}$ and $p_{y\,\mathrm{final}}$. Alternatively, it is possible to launch multiple classical trajectories in a Monte Carlo (CTMC) simulation, accounting for tunneling rates [21] and perpendicular momentum distributions at the tunnel exit [22]. In the latter approach, $p_{y\,\mathrm{final}}$ and θ [Fig. 1(b)] are extracted from the momentum distribution by Gaussian fits, in the same way as it is done for the experimental data. The simulations are launched for electric field strengths that were used in our experiment, returning the dependence of the final angle and of $p_{y\,\mathrm{final}}$ on intensity.

Figure 3 shows the results of the simulations, performed with helium at a fixed ellipticity value of 0.87. As a first observation we note that the nonadiabatic theory predicts a smaller intensity value as compared to the adiabatic prediction for the same final momentum $p_{y\,\mathrm{final}}$.

The relation between final momenta and intensity is a straightforward tool for intensity calibration of the experimental data, as proposed in [23,24]. From the measured value of $p_{y\,\mathrm{final}}$ using the mapping of Fig. 3 a value of intensity can be estimated, provided that one decides *a priori* whether to include nonadiabatic effects or not.

The attoclock [15,25], an angular streaking method using elliptically polarized light, is used to record photoelectron distributions or their corresponding ion momentum distributions. In a first set of experiments, presented in Fig. 4(a), we acquired helium ion momentum distributions with a COLd Target Recoil Ion Momentum Spectroscopy (COLTRIMS) apparatus [26] for different values of ellipticity at a constant intensity. Ultrashort laser pulses with a duration of about 7 fs at a central wavelength of 735 nm were generated by a Ti:sapphire amplifier system and focused into a supersonic gas jet target. By projecting final momenta with a small x component onto y, $p_{y\,\mathrm{final}}$ is obtained by a Gaussian fit.

At first glance, $p_{y\,\mathrm{final}}$ seems like a good observable to study the presence of nonadiabatic effects, since it is directly linked to an initial momentum offset as shown in Eq. (2). A direct test for nonadiabaticity would be to check whether an experimental scan of $p_{y\,\mathrm{final}}$ for different values of the Keldysh parameter agrees with semiclassical simulations over the same parameter range when an initial momentum offset different from zero, given by Eq. (1), is included.

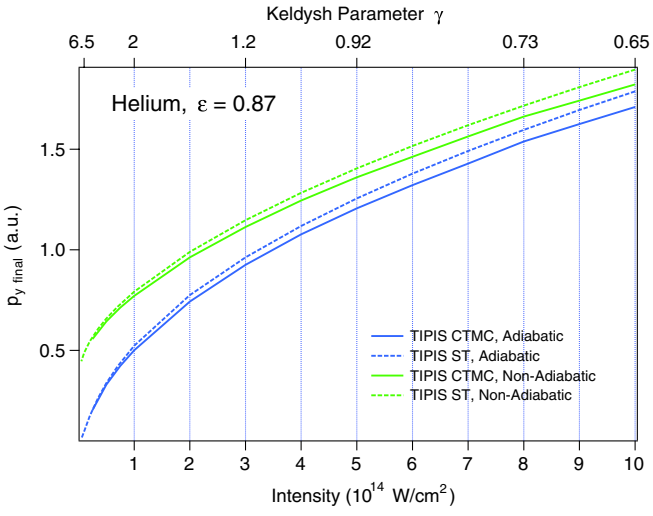

FIG. 3 (color online). Mapping of final momentum along the y axis, $p_{y\,\mathrm{final}}$, as a function of intensity. Single trajectory calculations (ST, dashed lines) and CTMC simulations (solid lines) are shown both in the case of zero initial momentum offset (blue) and with positive offset (green). Note the increased momentum, due to the offset, and the reduction in the CTMC calculations due to an out-of-phase ionization.

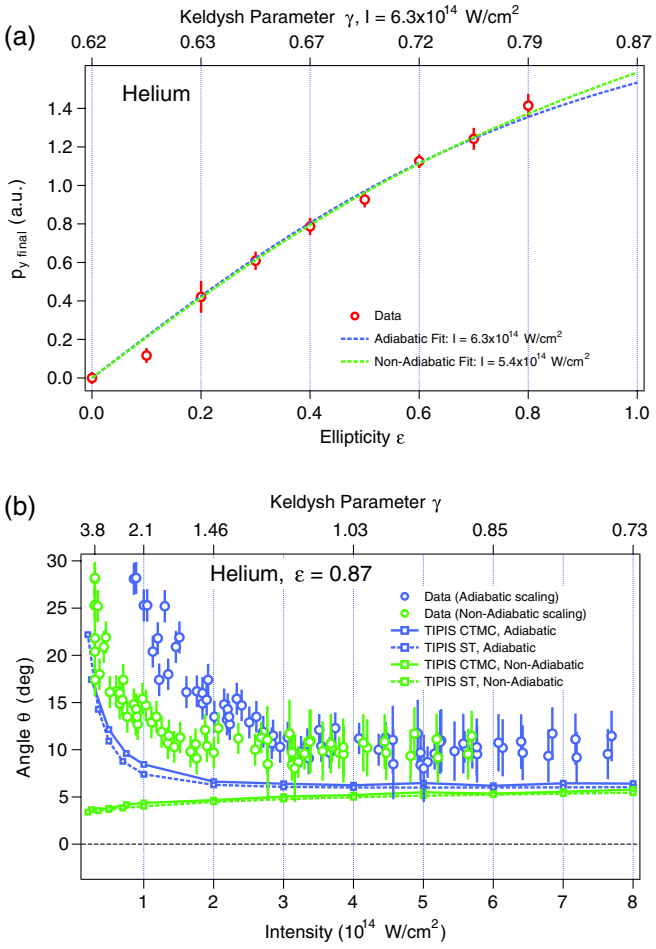

FIG. 4 (color online). (a) The analytical formula Eq. (2) with (dashed green line) and without (dashed blue line) the nonadiabatic contribution ($p_{y\,\mathrm{initial}}$ larger or equal to zero, respectively) is used to fit the ellipticity dependent data (red circles). (b) Final angle θ obtained from electron momentum distributions shown as a function of intensity together with the curves predicted by the TIPIS model with (green) and without initial offset (blue) for single trajectory calculations (ST, dashed lines) and CTMC calculations (solid lines). The intensities of the experimental data have been scaled according to the selected theory, following the mapping shown in Fig. 3.

However $p_{y\,\mathrm{final}}$ is also used to estimate *in situ* the intensity of the experimental data through the mapping shown in Fig. 3. This means that the same observable is used to calibrate the data as is used to test the theory used for the calibration. The problem of this approach becomes clear by having a look at Fig. 4(a), where we show the value of $p_{y\,\mathrm{final}}$ as a function of ellipticity at constant peak intensity I. By measuring the transmitted power through a rotating polarizer the orientation and ellipticity of the polarization are determined with a fit procedure before each measurement with a reproducible error below $\Delta\varepsilon = 0.01$ and $\Delta\theta = 1°$. The data in Fig. 4(a) can be fitted with the analytical formula of Eq. (2), leaving the electric field strength F as a free parameter. F is directly linked to the intensity by $F = \sqrt{I/(1+\varepsilon^2)}$, either with τ_0 larger or equal to zero, for the nonadiabatic or adiabatic approach, respectively. The result is that no conclusive statement about the observation of possible nonadiabatic effects can be drawn since both theories fit the experimental data reasonably well.

In order to overcome this dilemma, we select a different observable to test the validity of the nonadiabatic theory: the angle of the final momentum, defined by $\theta = \arctan(p_{x\,\mathrm{final}}/p_{y\,\mathrm{final}})$. This observable is maximally sensitive to the initial conditions at the exit point, thus to the initial velocity offset. Comparing the presented two scenarios, simulations show [Fig. 4(b)] that in the case of a nonadiabatic initial velocity offset, the angle θ decreases for smaller intensities, whereas in the case of no offset, θ increases. This is explained by the reduced Coulomb interaction in the proximity of the ion, due to the initial velocity offset. Therefore, the final angle of the electron momentum provides an observable where the two theories predict fundamentally different qualitative behavior and where we provide an experimental test that is independent of intensity calibration.

We tested the trend of the final angle θ as a function of intensity in a second set of experiments and compared it to the curves predicted with and without initial momentum offset in the y direction. The results are presented in Fig. 4(b). We set the ellipticity to be $\varepsilon = 0.87$ while varying the intensity of the laser pulses. In order to reach lower intensity values where nonadiabatic effects are predicted to be larger, we recorded the photoelectron momentum distributions with a velocity map imaging spectrometer (VMIS) [27], profiting from the high count rate provided by the increased density effusive target as compared to the gas jet of the COLTRIMS apparatus. As the momentum distribution exhibits no cylindrical symmetry and the polarization plane is oriented perpendicular to the detector of the VMIS, tomographic reconstruction is employed to obtain the full 3D momentum distribution [28,29] (further technical details are presented elsewhere [30]). Using the COLTRIMS, momentum distributions in helium for intensities below 4×10^{14} W/cm^2 are very difficult to achieve. For the high-intensity range instead, the corresponding ion momentum spectrum is recorded with the COLTRIMS detector.

This combination of measurements employing both COLTRIMS and VMIS permits an experiment spanning over a large range of intensities, from below 1×10^{14} to about 8×10^{14} W/cm^2, corresponding to a variation of the Keldysh parameter γ by more than a factor of 3, from 0.7 to 2.5. From radial and angular integration of the obtained momentum distributions, the radial momentum component $p_{y\,\mathrm{final}}$ and the final angle θ [Fig. 1(b)] are obtained by a Gaussian fit.

Figure 4(b) shows the experimental final angles plotted as a function of intensity for helium together with the curve predicted by the two-step TIPIS model either including or not an initial momentum offset (green and blue curves). The error bars in the angle result from uncertainty in determining the orientation of the major axis of the polarization, instrumental uncertainty, and statistical errors from the fitting of the momentum distribution.

To begin with, one notes the shift in intensity between the blue and green data points in Fig. 4(b) as a result of the different intensity calibration curves; see Fig. 3. Most importantly, it becomes clear that the theory including nonadiabatic effects fails at reproducing the trend of the data. Contrary to the fact that the final angle extracted from the experimental data increases for lower intensities, nonadiabatic theory predicts a decrement. On the other hand, the adiabatic theory reproduces qualitatively the experimental results. The additional offset between the data and the adiabatic theory in Fig. 4(b) is discussed elsewhere [31] by presenting a theory based on tunneling delay time. A full description would go beyond the scope of this work. Here, we want to emphasize that $p_{y\,\mathrm{final}}$ by itself, which is affected most directly by the proposed offset, would not have been sufficient to test the nonadiabatic theory, as demonstrated in Fig. 4(a). Only including $p_{x\,\mathrm{final}}$ and calculating the final angle θ allows for a conclusive statement. The Coulomb interaction in the proximity of the atom probes the initial state of the electron at its birth [32–34] and confers the information to the final state, measurable by the experiment. Furthermore, having two opposing trends allows for a strong statement without being sensitive to experimental uncertainties.

It is advantageous to use observables extracted from the peak of the Gaussian distribution, such as was done here, since these observables are minimally sensitive to noise. On the contrary, the approach of investigating the widths of the momentum distributions [6], while giving access to an initial momentum spread, will be affected by experimental noise, such as the thermal spread of ions and detector limitations, which might not be well quantified. Such additional spreads due to noise may falsely confirm nonadiabatic theories, which predict a larger momentum spread at the tunnel exit [12,14]. Thus, we believe that extracting the peak of the momentum distributions, rather

than the standard deviation, is best suited for observing nonadiabatic effects.

To summarize, we introduce a method to probe the electron wave packet properties at the tunnel exit. We then use it to investigate the initial momentum offset predicted by nonadiabatic theory, finding that our experimental data show no evidence of such offset. The good agreement of the adiabatic theory with our experimental trends suggests that the adiabatic model of tunnel ionization can be used for small intensities up to $\gamma = 2.5$. With larger γ, eventually, nonadiabatic effects are expected to emerge. However, our results suggest that the current nonadiabatic formalism [12,14,19] must be further developed to model experimental regimes with higher γ values properly.

This work was supported by both the NCCR Molecular Ultrafast Science and Technology (NCCR MUST), research instrument of the Swiss National Science Foundation (SNSF) and the ERC advanced Grant No. ERC-2012-ADG_20120216 within the seventh framework programme of the European Union. A. S. L. is supported by Marie Curie FP7 IIF Grant No. 275313. This project has been co-financed under FP7 Marie Curie COFUND.

*rboge@phys.ethz.ch

[1] P. B. Corkum, Phys. Rev. Lett. **71**, 1994 (1993).
[2] M. Y. Ivanov, M. Spanner, and O. Smirnova, J. Mod. Opt. **52**, 165 (2005).
[3] A. M. Perelomov, V. S. Popov, and M. V. Terentev, Sov. Phys. JETP **50**, 1393 (1966).
[4] L. V. Keldysh, Sov. Phys. JETP **20**, 1307 (1965).
[5] M. V. Ammosov, N. B. Delone, and V. P. Krainov, Sov. Phys. JETP **64**, 1191 (1986).
[6] L. Arissian, C. Smeenk, F. Turner, C. Trallero, A. V. Sokolov, D. M. Villeneuve, A. Staudte, and P. B. Corkum, Phys. Rev. Lett. **105**, 133002 (2010).
[7] A. N. Pfeiffer, C. Cirelli, M. Smolarski, D. Dimitrovski, M. Abu-samha, L. B. Madsen, and U. Keller, Nat. Phys. **8**, 76 (2012).
[8] M. Meckel *et al.*, Science **320**, 1478 (2008).
[9] H. Akagi, T. Otobe, A. Staudte, A. Shiner, F. Turner, R. Dörner, D. M. Villeneuve, and P. B. Corkum, Science **325**, 1364 (2009).
[10] L. Holmegaard *et al.*, Nat. Phys. **6**, 428 (2010).
[11] J. Maurer, D. Dimitrovski, L. Christensen, L. B. Madsen, and H. Stapelfeldt, Phys. Rev. Lett. **109**, 123001 (2012).
[12] V. D. Mur, S. V. Popruzhenko, and V. S. Popov, J. Exp. Theor. Phys. **92**, 777 (2001).
[13] G. L. Yudin and M. Y. Ivanov, Phys. Rev. A **64**, 013409 (2001).
[14] I. Barth and O. Smirnova, Phys. Rev. A **84**, 063415 (2011).
[15] P. Eckle, A. N. Pfeiffer, C. Cirelli, A. Staudte, R. Dörner, H. G. Muller, M. Büttiker, and U. Keller, Science **322**, 1525 (2008).
[16] D. I. Bondar, Phys. Rev. A **78**, 015405 (2008).
[17] I. Dreissigacker and M. Lein, Chem. Phys. **414**, 69 (2013).
[18] D. Shafir, H. Soifer, B. D. Bruner, M. Dagan, Y. Mairesse, S. Patchkovskii, M. Yu. Ivanov, O. Smirnova, and N. Dudovich, Nature (London) **485**, 343 (2012).
[19] S. P. Goreslavski, G. G. Paulus, S. V. Popruzhenko, and N. I. Shvetsov-Shilovski, Phys. Rev. Lett. **93**, 233002 (2004).
[20] N. I. Shvetsov-Shilovski, D. Dimitrovski, and L. B. Madsen, Phys. Rev. A **85**, 023428 (2012).
[21] X. M. Tong and C. D. Lin, J. Phys. B **38**, 2593 (2005).
[22] N. B. Delone and V. P. Krainov, J. Opt. Soc. Am. B **8**, 1207 (1991).
[23] A. S. Alnaser, X. Tong, T. Osipov, S. Voss, C. Maharjan, B. Shan, Z. Chang, and C. Cocke, Phys. Rev. A **70**, 023413 (2004).
[24] C. Smeenk, J. Z. Salvail, L. Arissian, P. B. Corkum, C. T. Hebeisen, and A. Staudte, Opt. Express **19**, 9336 (2011).
[25] P. Eckle, M. Smolarski, P. Schlup, J. Biegert, A. Staudte, M. Schöffler, H. G. Muller, R. Dörner, and U. Keller, Nat. Phys. **4**, 565 (2008).
[26] J. Ullrich, R. Moshammer, A. Dorn, R. Dörner, L. Ph. H. Schmidt, and H. Schmidt-Böcking, Rep. Prog. Phys. **66**, 1463 (2003).
[27] A. T. J. B. Eppink and D. H. Parker, Rev. Sci. Instrum. **68**, 3477 (1997).
[28] M. Wollenhaupt, M. Krug, J. Köhler, T. Bayer, C. Sarpe-Tudoran, and T. Baumert, Appl. Phys. B **95**, 647 (2009).
[29] C. Smeenk, L. Arissian, A. Staudte, D. M. Villeneuve, and P. B. Corkum, J. Phys. B **42**, 185402 (2009).
[30] M. Weger, J. Maurer, A. Ludwig, L. Gallmann, and U. Keller, arXiv:1306.6280.
[31] A. S. Landsman, M. Weger, J. Maurer, R. Boge, A. Ludwig, S. Heuser, C. Cirelli, L. Gallmann, and U. Keller, arXiv:1301.2766v2.
[32] A. N. Pfeiffer, C. Cirelli, A. S. Landsman, M. Smolarski, D. Dimitrovski, L. B. Madsen, and U. Keller, Phys. Rev. Lett. **109**, 083002 (2012).
[33] C. Hofmann, A. S. Landsman, C. Cirelli, A. N. Pfeiffer, and U. Keller, J. Phys. B **46**, 125601 (2013).
[34] A. S. Landsman, A. N. Pfeiffer, C. Hofmann, M. Smolarski, C. Cirelli, and U. Keller, New J. Phys. **15**, 013001 (2013).